Clustering of inertial spheres in evolving Taylor-Green vortex flow

Rohith Jayaram,[1] Yucheng Jie,[2] Lihao Zhao,[2,1,*] and Helge I. Andersson[1]

[1] *Department of Energy and Process Engineering, Norwegian University of Science and Technology, Trondheim 7491, Norway*

[2] *AML, Department of Engineering Mechanics, Tsinghua University, Beijing 100084, China*

Abstract

Clustering of inertial spheres in a statistically unsteady flow field is believed to be different from particle clustering observed in statistically steady flows. The continuously evolving three-dimensional Taylor-Green vortex (TGV) flow exhibits time-varying length- and time-scales, which are likely to alter the resonance of a given particle with the evolving flow structures. The tendency of homogeneously introduced spherical point-particles to cluster preferentially in the TGV flow is observed to depend on the particle inertia, parameterized in terms of the particle response time τ_p. The degree of the inhomogeneity of the particle distribution is measured by the variance σ^2 of Voronoï volumes. The time evolution of the particle-laden TGV-flow is characterized by a viscous dissipation time scale τ_d and the effective Stokes number $St_{eff} = \tau_p/\tau_d$. Particles with low/little inertia do not cluster in the early stage when the TGV-flow only consists of large-scale and almost inviscid structures and $St_{eff} < 1$. Later, when the large structures have been broken down to smaller vortices, the least inertial particles exhibit a stronger preferential concentration than the more inertial spheres. At this stage, when the viscous energy dissipation has reached its maximum level, the effective Stokes number of these particles have reached the order of one. Particles are generally seen to cluster preferentially at strain-rate dominated locations, i.e. where the second invariant Q of the velocity gradient tensor is negative. However, a memory effect can be observed in the course of the flow evolution where high σ^2-values do not always correlate with $Q < 0$.

I. INTRODUCTION

The Taylor-Green vortex (TGV) flow first considered by Taylor and Green [1] is one of the classic flow systems used to study vortex dynamics, transition, energy dissipation and decay processes [2, 3], including excitations at smaller scales and the resulting decaying turbulence [4]. The TGV flow starts as a regular array of large-scale vortices, which are scrambled, i.e. bended and stretched, by non-linear inertia, and eventually turned into quasi-homogeneous small-scale turbulence subjected to viscous dissipation; see e.g. Brachet [4] and Sharma and Sengupta [5]. Besides being an appreciated flow system for studies of intricate unsteady vortex dynamics and decaying turbulence, the TGV flow also represents an attractive benchmark for testing and verification of numerical schemes [2, 6].

* E-mail address: zhaolihao@mail.tsinghua.edu.cn

Dilute suspensions of particles in turbulent flows have been extensively studied with the view to better understand particle transport, dispersion and preferential concentration. Different flow systems are adopted, notably homogenous isotropic turbulence (HIT) and turbulent channel flows. By means of a point-particle approach, Squires and Eaton [7] and Calzavarini et al. [8] studied clustering of spherical particles in HIT. Similarly, Marchioli and Soldati [9], Nilsen et al. [10] and Yuan et al. [11] examined particle clustering in channel flow turbulence. A common feature of these flows is the statistical steadiness, which implies that the characteristic length and time scales are independent of time. Nevertheless, the flow scales seen by a particle along its trajectory do change in the wall-normal direction. The Kolmogorov scale for time, for instance, increases fivefold from the near-wall region to the channel center at a friction Reynolds number 180 [12]. However, an inertial particle is primarily driven in the direction of the bulk flow, whereas major wall-normal excursions are rare. Therefore, the vast majority of particles takes a long time to drift across different regions of the flow and to interact with different length and time scales. In the evolving TGV-flow, however, the characteristic scales of the flow constantly change with time and particles all over the flow are immediately exposed to the varying time scales. This variation is likely to alter the resonance of a given inertial particle with the gradually evolving flow structures.

Steady-state TGV flows have been considered in several earlier studies to explore various aspects of particle additives in vortical flows, of which the papers by Maxey [13], Wang et al. [14], Durham et al. [15], Yao and Capecelatro [16] and Ruan et al. [17] are representative examples. Bergougnoux et al. [18] set up a model experiment using electro-convection to mimic such a two-dimensional array of steady vortices. Initially, however, Stommel [19] used the two-dimensional TGV flow as a model for cellular vortex flow to study plankton behavior in Langmuir circulations [20] in oceans and lakes. The investigation by Durham et al. [15] on gyrotactic motility in steady TGV flow suggested that the vortical flow might be able of efficiently separating species with different motility characteristics. Phytoplankton is an essential ingredient in aquatic ecosystems and their motion in the oceanic environment affects their feeding abilities and thus the potential for phytoplankton blooming; see e.g. the review articles by Durham and Stocker [21] and Guasto et al. [22]. Another marine occurrence of particle-laden flows is microplastic pollution, which has recently grown to become of major environmental concern, as address for instance by Hidalgo-Ruz et al. [23]

and Barboza and Gimenez [24]. Microplastics are transported by currents and tides, which are turbulent on the relevant scales of the microplastic particles (Galloway et al. [25]). The density of microplastics, which is affected by weathering and biofouling, determines whether the microplastics will float near the sea surface or sediment at the seabed [26–28].

The dynamical behavior of pollutant microplastics and aquatic micro-organisms in the ocean can be modelled as a dilute suspension of microparticles in a vortical flow field. The steady-state TGV flow [1], which appears as an array of counterrotating vortices, represents a tractable starting point. However, the unsteady TGV flow [2–6], which rapidly develops into a three-dimensional and time-varying flow field, represents a far more realistic model of oceanic turbulence characterized by constantly varying vortex structures. In spite of the abundant interest in the time-dependent TGV flow as a benchmark case [29], for instance at the 1st International Workshop on High-Order CFD Methods at the 50th AIAA Aerospace Science Meeting in 2012, particle behavior in unsteady TGV flows has apparently not been dealt with before.

Similarly as the turbulent Kolmogorov flow, e.g. De Lillo et al. [30], the evolving TGV flow appears as an attractive flow field in which one can assess whether or not the well-established knowledge on particle clustering in steady-state flows carries over to flow fields in which the flow scales change continuously with time. Unlike the periodic Kolmogorov flow, however, the characteristic length and time scales vary aperiodically throughout the evolution of the TGV flow. One can therefore anticipate that a particle with given inertia will respond differently to the typical vortical flow structures during the flow evolution since the characteristic time scale of the unsteady TGV-flow gradually changes with time. Moreover, even though the viscous drag force on a particle at a given time is determined by the local flow conditions at that time, particle inertia may give rise to a certain memory effect, which in turn may induce a decorrelation of the particle clustering from the vortical structures.

In order to explore particle clustering in the evolving TGV-flow, we adopt an Eulerian-Lagrangian approach, in which the unsteady flow field is obtained by integration of the three-dimensional Navier-Stokes equations. Tiny equal-sized spherical particles are subjected only to Stokes-drag when tracked in the evolving flow field. In order to examine the influence of inertia on particle clustering, a wide range of particle densities is considered.

The Voronoï-volume approach will be employed to quantify the particle clustering. This method was first used to describe the clustering of galaxies by van de Weygaert and Icke [31].

Monchaux et al. [32] described the Voronoï-volume approach to quantify particle clustering in turbulent flows and also discussed its advantages over other methods. This approach has recently received wide usage in particle-laden flows. One Voronoï-cell is defined as the ensemble of points that are closer to a particular particle than to any other particle [32]. From the very definition, the inverse of the Voronoï-cell represents the local particle concentration. Monchaux et al. [33] used this approach to quantify the clustering of inertial particles in HIT. Many recent works, such as Nilsen et al. [10], Yuan et al. [11], and Garcia-Villalba et al. [34], have used this approach in different flow systems.

The local topology of the flow field can be categorized by means of the second invariant of the velocity gradient tensor, as suggested by Hunt et al. [35]. More specifically, the sign of the invariant distinguishes between rotation-rate and strain-rate dominance. Inertial particles seem to have an inclination to reside in strain-rate dominated regions; e.g. Balachandar and Eaton [36], Sundaram and Collins [37], and Bec et al. [38]. In the present study, the second invariant will be examined along with the concentration field (i.e. the reciprocal Voronoï-volume) in order to explain the preferential clustering.

The article is organized as follows. Section 2 presents the governing flow and particle equations along with a brief account of Voronoï-tessellation. Section 3 provides a series of global and local results aimed to elucidate particle clustering from different perspectives, before the conclusions are summarized in Section 4.

II. METHODOLOGY

A. Eulerian fluid dynamics

We consider the unsteady TGV flow in a cubical box with sides $2\pi L$, similarly as in the studies by DeBonis [2] and Brachet et al. [3]. The three-dimensional and incompressible fluid motion is governed by the conservation equations for mass and momentum:

$$\frac{\partial u_i}{\partial x_i} = 0 \tag{1}$$

$$\rho(\frac{\partial u_i}{\partial t} + u_j \frac{\partial u_i}{\partial u_j}) = -\frac{\partial p}{\partial x_i} + \mu \frac{\partial^2 u_i}{\partial x_j \partial x_j}, \tag{2}$$

where p is the pressure and u_i denotes the velocity component in the x_i-direction of a Cartesian coordinate system. The Newtonian fluid has density ρ and dynamic viscosity μ.

Gravity is not included in our study. It should be noticed that the flow field is unaffected by the presence of particle additives. The assumption of one-way coupling between the fluid and particle phases is justified for sufficiently dilute suspensions.

Initial conditions for the three components of the velocity vector at $t = 0$ are set in accordance with DeBonis [2] as:

$$u = V_0 sin(\frac{x}{L})cos(\frac{y}{L})cos(\frac{z}{L}) \tag{3}$$

$$v = 0 \tag{4}$$

$$w = -V_0 cos(\frac{x}{L})cos(\frac{y}{L})sin(\frac{z}{L}), \tag{5}$$

where V_0 and L are initial scales of velocity and length. The vorticity vector of the two-componential flow field in equations (3 - 5) is entirely in the y-direction and illustrated in figure 1.

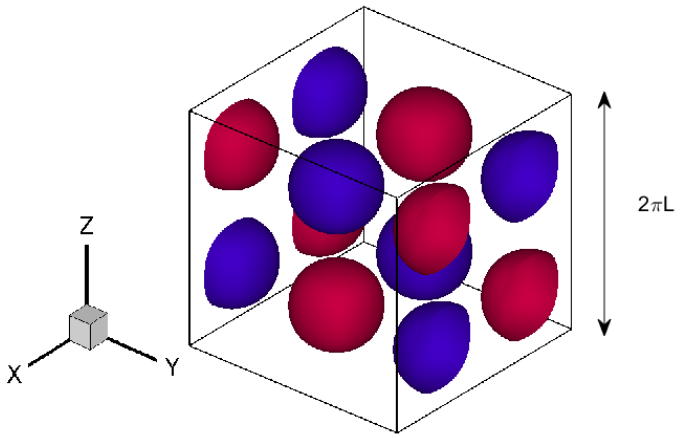

FIG. 1: The initial flow field illustrated by means of iso-surfaces of $\omega_y = \partial u/\partial z - \partial w/\partial z$ in the cubic domain. The colors distinguish between positive (red) and negative (blue) values of ω_y.

The governing equations (1, 2) are integrated on a three-dimensional mesh with 128^3 equally spaced grid points over the computational volume $V_d = (2\pi L)^3$, starting from the initial field in equations (3 - 5), using periodic boundary conditions in all three coordinate directions. The Reynolds number $Re = \rho V_0 L/\mu$ is set to 1600, just as in the study by Brachet [4]. With $Re \gg 1$, non-linear inertia is essential in the flow development.

A pseudo-spectral method is used to compute spatial derivatives in x- and y-directions, whereas second-order central-differences approximate the spatial derivatives in the z-

direction. The time advancement is carried out by using an explicit second-order Adams-Bashforth scheme. The velocity at the new time level is obtained by a standard projection method in which the Poisson equation is solved using the Sherman-Morrison algorithm [39]. The resulting Navier-Stokes solver was verified in our recent article by Jayaram et al. [40].

B. Lagrangian particle dynamics

Spherical point-particles are suspended in the TGV flow and the individual particles are tracked using a Lagrangian approach. The translational motion of an inertial sphere is governed by Newton's second law of motion:

$$m\frac{\mathrm{d}v_i}{\mathrm{d}t} = F_i, \tag{6}$$

where $v_i = \mathrm{d}x_i/\mathrm{d}t$ is the translational particle velocity vector and F_i is the force acting on the particle. The mass of a spherical particle with density ρ_p is $m = 4\pi a^3\rho_p/3$, where a is the particle radius. The inertial particles are assumed to be sufficiently small so that only the Stokesian drag force

$$F_i = 6\pi\mu a(u_{p,i} - v_i) \tag{7}$$

is taken into account. Particles that satisfy neglection of other forces than viscous drag are referred to as Heavy Inertial Particles (HIP), e.g. Mitra et al. [41]. This approximation can be justified for density ratios $D \gg 1$, where D is the ratio between the particle density ρ_p and the fluid density ρ. According to equation (7), the viscous force on a particle from the surrounding fluid is proportional to the slip velocity $\Delta u_i = u_{p,i} - v_i$, i.e. the difference between the fluid velocity at the particle position $u_{p,i}$ and the particle velocity v_i. The expression (7) is formally valid only in the creeping flow limit where the particle Reynolds number $Re_p = 2a|\Delta u_i|\rho/\mu$ goes to zero. Several modifications exist for finite particle Reynolds numbers. Here, we adopt a simple non-linear correction

$$F_i = 6\pi\mu a(u_{p,i} - v_i)(1 + 0.15Re_p^{0.687}) \tag{8}$$

suggested by Schiller and Naumann [42]. The modified expression for the drag force in equation (8) is accurate up to $Re_p \approx 1000$. We verified a posteriori that the volume-averaged

particle Reynolds number Re_p remained well below 10, except for the $St = 100$ particles for which maximum value of about 11 was reached at $t \approx 4V_0/L$. Now, by combining (6) and (8) we arrive at the final form of the governing equation for the translational motion of a spherical particle

$$\frac{\mathrm{d}v_i}{\mathrm{d}t} = \frac{1}{\tau_p}(u_{p,i} - v_i)(1 + 0.15Re_p^{0.687}), \tag{9}$$

where $\tau_p = 2a^2D/9\nu$ is the particle response time which is a dimensional measure of how effectively a particle adjusts to the local flow field. By means of the time scale $\tau_f = L/V_0$ of the initial flow field, we define the nominal Stokes number St as the ratio τ_p/τ_f.

Ordinary differential equations (9) for each and every particle are integrated forward in time by means of a second-order Adams-Bashforth scheme using the same time step as for the fluid equations (1, 2). A second-order quadratic interpolation scheme is used to obtain the fluid velocity at particle location. The same Lagrangian particle tracking algorithm has been used in earlier papers by Mortensen et al. [43] and Zhao et al. [44, 45] on particle-laden channel flow.

The aim of the present work is to investigate how inertial spheres cluster in the TGV flow. The evolving TGV flow enables us to explore how the spheres are responding to the non-monotonic variation of the relevant time scale of the vortical flow field. We consider a wide range of inertial spheres with Stokes number St varying from 0.1 to 100, i.e. spanning three decades. The equal-sized spheres with radius $a = 0.005L$ have density ratios D in the range from 11.25 at $St = 0.1$ to 11250 at $St = 100$. For each nominal Stokes number St, $N_p = 10^5$ particles are fed at random positions into the TGV flow at $t = 0$. The use of periodic boundary conditions at all sides of the computational box assures that the number of particles is maintained throughout the simulation.

C. Voronoï tessellation

Voronoï-diagrams represent a practical tool to quantify clustering of particles in a flow field; see e.g. Monchaux et al. [32]. A Voronoï diagram is the unique decomposition of a nD space into independent cells associated to each particle. One Voronoï cell includes all the space that is closer to one particular particle than to any other [33]. The whole computational domain can be divided into sub-volumes based on the Voronoï volumes. Any

open Voronoï cells at the boundaries are taken care of by mirrored ghost particles which ensure that all sub-volumes at the boundaries of the domain are closed [11]. An outcome of 2D Voronoï tessellation is illustrated in figure 2. $St = 1$ particles are dispersed in the TGV flow and the distribution of Voronoï cells in the horizontal mid-plane at time $t = 5\tau_f$ gives an indication of how the particles are unevenly distributed. Since the area of each individual cell is a measure of the distance to the nearest neighbors, small Voronoï areas correspond to high local concentrations and vice versa. The most densely populated areas appear as the darkest in the plot. Notice the symmetric particle distributions about $x = \pi L$ and about $y = \pi L$ in figure 2, which are leftovers from the symmetries of the initial flow field.

The volume of each Voronoï cell is normalized by the mean computational volume per particle V_d/N_p, where V_d is the volume of the cubic computational domain. The Voronoï volume V_k associated with the kth particle is normalized as $V_k N_p/V_d$. Now, since $\sum_{k=1}^{N_p} V_k = V_d$ it follows that the average value of all the normalized Voronoï volumes is $\bar{V} = \frac{1}{N_p}\sum_{k=1}^{N_p} V_k N_p/V_d = 1$. Similarly, in 2D cases, 2D Voronoï volumes are normalized with the corresponding computational area and the number of particles in the slice.

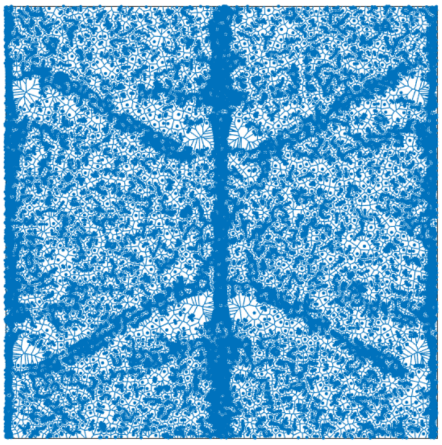

FIG. 2: Illustration of Voronoï cells (i.e. 2D volumes) for $St = 1$ particles in the horizontal (x,y)-midplane at $z = \pi L$ at time $t = 5$. Hereinafter, t stands for the dimensionless time $t/\tau_f = tV_0/L$.

III. RESULTS AND DISCUSSION

A. Evolving Taylor-Green vortex flow simulation

The unsteady Navier-Stokes equations (1, 2) were integrated in time and three-dimensional space, starting from the two-componential initial field (3 - 5) at Reynolds number $Re = 1600$ based on the initial velocity and length scales V_0 and L. The time evolution of the volume-averaged kinetic energy:

$$E_k = \int_{V_d} \frac{u_i u_i}{2} dV, \tag{10}$$

is shown in figure 3(a). The corresponding volume-averaged energy dissipation rate can be seen in figure 3(b), where the particular notation $\epsilon(E_k)$ emphasizes that ϵ is deduced from the decay rate of the kinetic energy according to:

$$\epsilon(E_k) = -\frac{\mathrm{d}E_k}{\mathrm{d}t}. \tag{11}$$

The volume-averaged energy dissipation can alternatively be obtained as the local viscous energy dissipation rate $\nu(\frac{\partial u_i}{\partial x_j})(\frac{\partial u_i}{\partial x_j})$ integrated over the computational domain V_d. However, due to the persistent periodicity of the flow field over the computational domain, the volume-averaged energy production and transport (i.e. convection and diffusion) terms vanish and the volume-averaged kinetic energy equation simplifies to the balance equation (11).

The present results follow the same characteristic trends as already reported by DeBonis [2] and Dairay et al. [6], namely a monotonic decay of the kinetic energy E_k, whereas the energy dissipation rate $\epsilon(E_k)$ first increases until it peaks around $t = 9$ and thereafter decays. The modest deviations between the present solution and the reference solutions are comparable with the grid resolution effects observed when the grid size was increased from 128^3 to 512^3; see DeBonis [2]. Recall that the present computer code has spectral accuracy only in two directions, whereas the finite-difference discretization in the z-direction is second-order accurate [40].

The non-monotonic variation of the energy dissipation rate in figure 3(b) can be explained in terms of the alterations of the vortex structures as the time evolves, as discussed for instance by Brachet et al. [3], DeBonis [2] and Sharma and Sengupta [5]. Here, we follow DeBonis [2] and show three-dimensional views of ω_y at six distinct time levels from $t = 3$

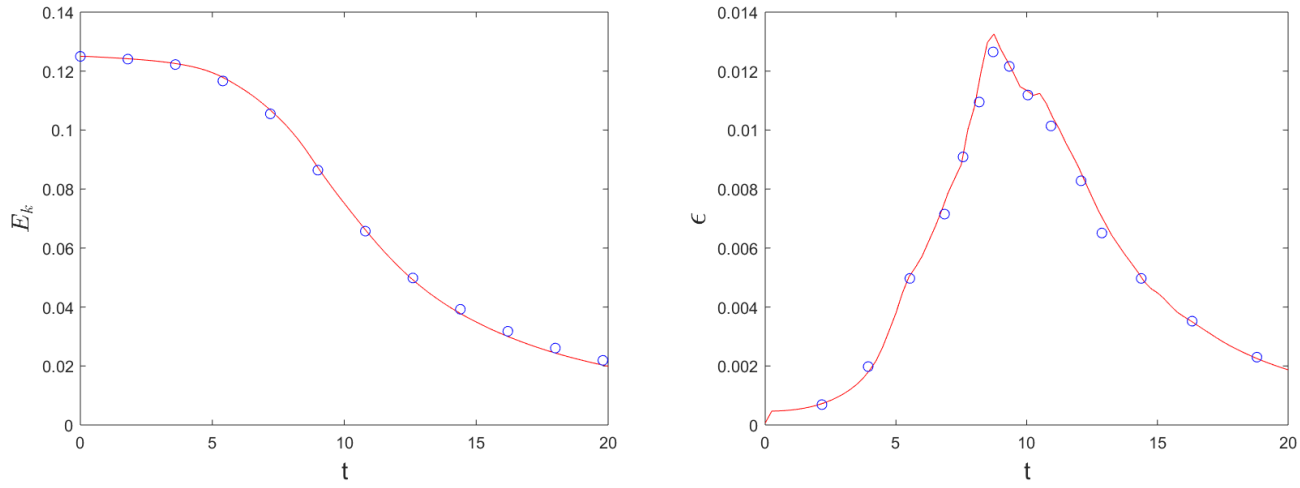

(a) (b)

FIG. 3: (a) Evolution of the volume-averaged kinetic energy E_k compared with DeBonis [2] and (b) the energy dissipation rate $\epsilon(E_k)$ compared with Dairay et al. [6]. The reference solutions are marked by circles.

to $t = 15$ in figure 4. The flow is essentially inviscid at $t = 3$ and the smooth iso-surfaces reflect the regular vortex structures. Non-linear effects, e.g. vortex stretching and bending, are altering the vortices in the early stages of the evolution of the flow. As the size of the vortex structures gradually diminishes with time, the viscous energy dissipation increases monotonically until $t \approx 9$. However, since no energy is fed into the flow system, $\epsilon(E_k)$ eventually starts to decay alongside with the decay of the volume-averaged kinetic energy E_k. The monotonous decay of the turbulence-like vortices is primarily caused by viscous action and the smaller-scale flow structures at $t = 15$ resemble homogeneous isotropic turbulence.

The time evolution of the TGV flow makes it tempting to explore how inertial particles will disperse and cluster in this statistically unsteady flow field. The characteristic scales of the TGV flow are continuously changing with time. The length scale of the vortical flow structures reduces with time (see figure 4), whereas the viscous dissipation time scale $\tau_d = (\nu/\epsilon)^{\frac{1}{2}}$ shortens until $t \approx 9$ (see figure 3b) and thereafter increases as time goes on. The nominal Stokes number St, which is based on the initial flow time scale $\tau_f = L/V_0$, is therefore believed to be of physical relevance only in the very early stage of the flow evolution.

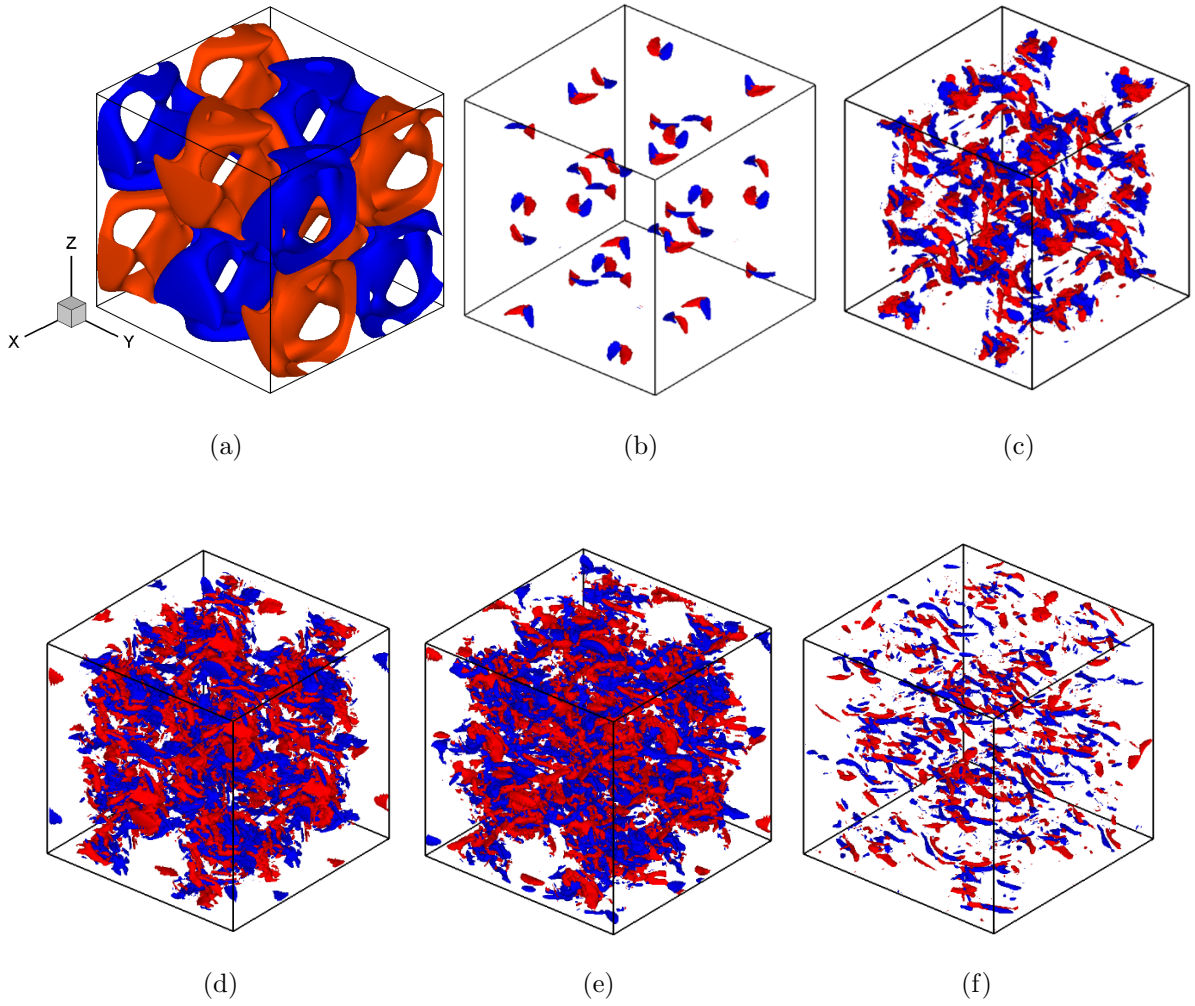

FIG. 4: Perspective view of the time evolution of ω_y iso-surfaces. The colors distinguish between positive (red) and negative (blue) surfaces. (a) $t = 3$, almost inviscid vortices; (b) $t = 5$, vortex roll-up; (c) $t = 7$, change of structure; (d) $t = 9$, coherence breakdown; (e) $t = 11$, turbulence-like; (f) $t = 15$, decaying turbulence.

B. Clustering of particles

Eight swarms of different particles were initialized at random positions throughout the computational domain at the start of the flow computation at $t = 0$. The initially homogeneously distributed particles were tracked in the gradually evolving flow field and experienced an unmixing depending crucially on particle inertia.

1. *Unmixing*

The variance σ^2 of the Voronoï-volumes V_k is adopted as a measure of the inhomogeneity of the particle distribution in the computational box. The time evolution of σ^2 presented in figure 5 shows the effect of particle inertia on the tendency of the particles to unmix, i.e. the different inhomogeneities of the particle distributions reflect the particles' tendency to concentrate preferentially in the flow field. The qualitatively different trends observed in figure 5 may suggest that the particles can be categorized in three different groups, each with their own characteristic response to the evolving flow field.

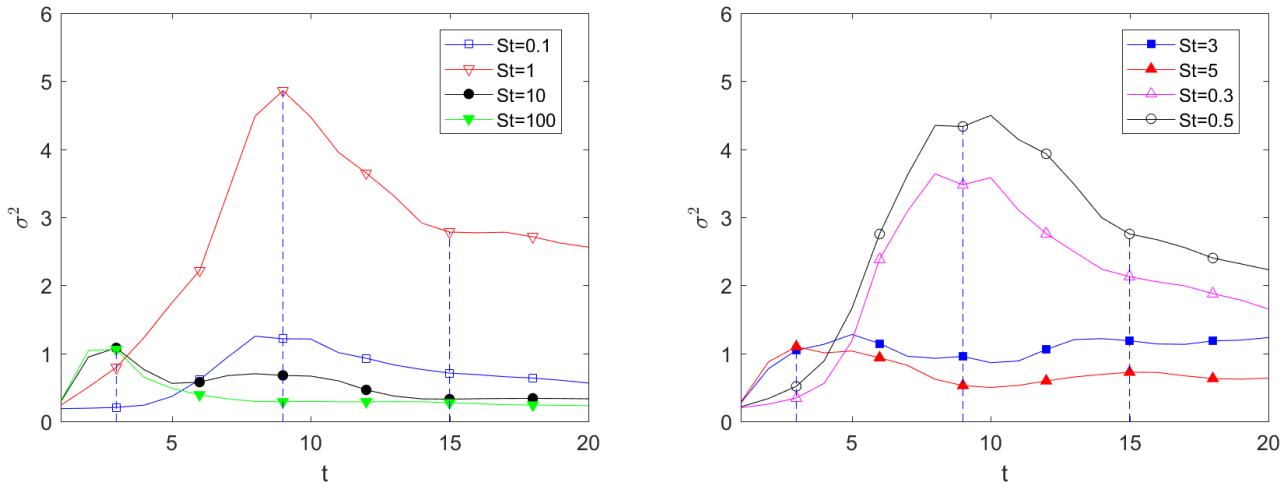

(a) (b)

FIG. 5: Time evolution of the variance σ^2 of the Voronoï-volumes for different nominal Stokes numbers St. The Voronoï volumes V_k are normalized by the volume V_d of the computational box and the number of particles N_p. (a) $St = 0.1, 1, 10, 100$ and (b) $St = 0.3, 0.5, 3, 5$. The vertical lines indicate the particular time levels $t = 3, 9$ and 15, which correspond to panels a, d and f in figure 4.

Particles having nominal Stokes number $St \leq 1$ exhibit only modest inhomogeneities in the early stages of the flow and σ^2 is lower than for any of the more inertial particles $St > 1$ at $t = 3$, i.e. as long as the flow is almost inviscid. As time goes on, however, σ^2 increases for the $St \leq 1$ particles and reaches a maximum level around $t = 9$. These particles with modest inertia are strongly clustered when the kinetic energy dissipation rate is maximized, contrary to the more inertial particles ($St > 1$) which homogenize as the time

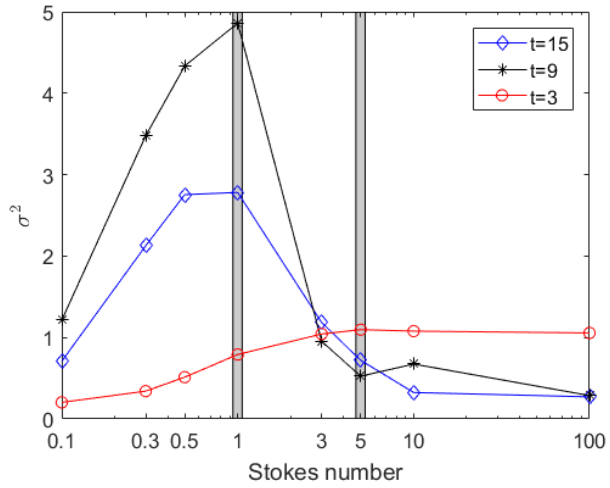

FIG. 6: Dependence of the variance σ^2 as a function of nominal Stokes number St at three qualitatively different stages of the flow development, namely $t = 3$ (see figure 4a); $t = 9$ (see figure 4d); $t = 15$ (see figure 4f). The three qualitatively different Stokes number groups are demarcated by vertical bands.

increases from $t = 3$ to 9. The $St \leq 1$ particles are seen to mix after the energy dissipation has reached its maximum level, whereas particles with intermediate inertia ($St = 3$ and 5) are seen to unmix, i.e. σ^2 increases with time. In contrast, the most inertial spheres with $St \geq 10$ exhibit stronger clustering than particles with lower inertia at $t = 3$, but maintain only a modest degree of preferential concentration from $t = 9$ and further throughout the simulation.

The results in figure 5 seem to suggest that the time evolution of the particle clustering can be divided into three qualitatively different stages. The variance σ^2 has therefore been plotted in figure 6 at the three distinct time levels $t = 3$ (almost inviscid flow), $t = 9$ (maximum energy dissipation), and $t = 15$ (turbulence-like eddies). Along with the variance σ^2 of the Voronoï volumes, the corresponding probability density function (p.d.f.) of the Voronoï-volumes at the same three time levels are shown in figure 7.

The flow is still essentially inviscid at $t = 3$ and the p.d.f.s in figure 7(a, b) show beyond any doubt that the $St = 0.1$ particles are almost randomly distributed in the flow field since their p.d.f. closely matches a Poisson distribution, which is the signature of evenly distributed particles. Even though the p.d.f.s of the other particles with $St \leq 1$ deviate from the Poisson distribution, these particles are yet less clustered than the more inertial

particles. This is consistent with the finding that σ^2 is lower for $St \leq 1$ than for $St > 1$ particles in the early stages of the simulation, as concluded from figures 5 and 6.

The TGV flow has undergone substantial changes due to non-linear vortex bending and stretching and viscous stresses act to promote the energy dissipation at $t = 9$. All particles now exhibit preferential concentration, as shown by the p.d.f.s in figure 7 (c, d), which all deviate from the Poisson distribution. The largest deviations are observed for the $St \leq 1$ particles, which reflect a stronger clustering of the least inertial particles.

The situation has changed at time $t = 15$ when a turbulence-like dissipative flow prevails. The p.d.f.s in figures 7(e, f) show that the most inertial particles now are closest to the Poisson distribution, i.e. to a random distribution. This is indeed consistent with the relatively low variance σ^2 for $St = 10$ and 100 seen in figures 5(a) and 6.

2. The effective Stokes number

The velocity and length scale of the initial flow field, V_0 and L, have physical relevance only in the early stages of the flow development. Also the corresponding time scale $\tau_f = L/V_0$ soon loses its relevance. It is evident from the snapshots in figure 4 that the characteristic scales of the TGV flow are varying as the flow is evolving. We therefore introduce the viscous dissipation time scale $\tau_d = (\nu/\epsilon)^{\frac{1}{2}}$, where ϵ is the local energy dissipation rate. τ_d has the same form as the so-called Kolmogorov time scale characteristic of small-scale turbulence. We now claim that the same time scale can be employed even at intermediate stages of the flow development, e.g. around $t = 9$, although the TGV flow is far from being fully turbulent. Since the TGV flow appears as quasi-homogeneous in space, we rely on the volume-averaged dissipation rate $\epsilon(E_k)$ defined in equation (11). We are now in the position to define an effective Stokes number

$$St_{eff} = \tau_p/\tau_d = St \cdot \tau_f/\tau_d. \tag{12}$$

While the nominal Stokes number St is constant, the time scale ratio τ_f/τ_d varies continuously due to the time variation of the viscous energy dissipation $\epsilon(E_K)$ in figure 3(b). The time-varying effective Stokes number defined in equation (12) is believed to be of better physical relevance with respect to clustering of inertial particles than the nominal Stokes number St used to classify the different particles.

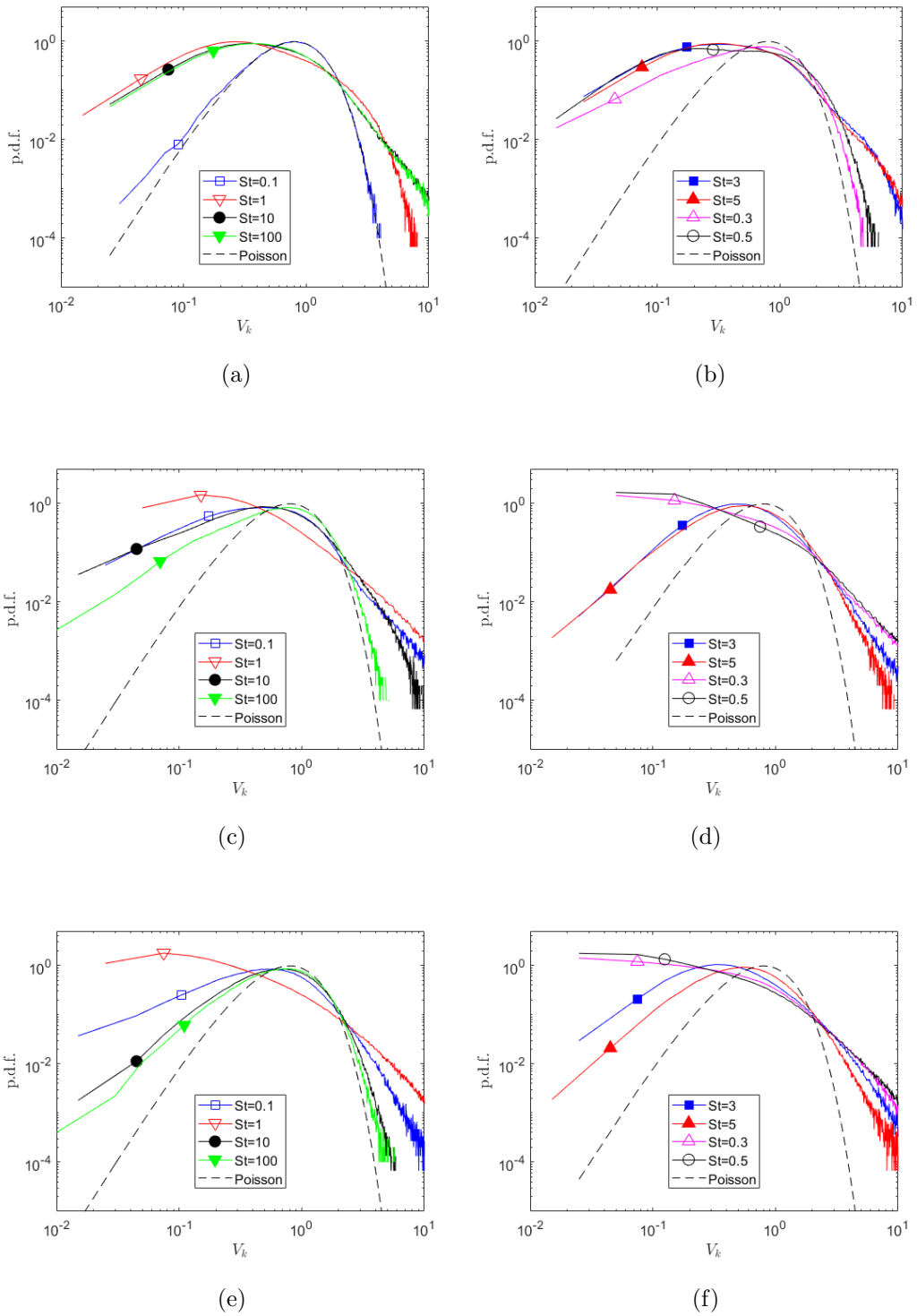

FIG. 7: Probability density functions of normalized Voronoï volumes at (a, b) t = 3; (c, d) t = 9; and (e, f) t = 15, cf figure 6. The broken line is the Poisson distribution given by Ferenc and Néda [46].

The time evolution of the effective Stokes number St_{eff} is shown in figure 8, from which it can be observed that St_{eff} first increases until $t \approx 9$ and thereafter decreases with time. These trends are the same for all nominal Stokes numbers St and are a direct consequence of the flow time scale τ_d being inversely proportional with $\epsilon^{\frac{1}{2}}$.

In the earliest stages of the simulation, the TGV flow remains essentially inviscid and the large-scale TG vortices are clearly recognizable at $t = 3$ in figure 4(a). The least inertial particles with nominal Stokes number $St = 0.1$ are almost randomly distributed (see figure 7a), whereas the amount of clustering increases monotonically with St, as shown in figure 6. The changeover from almost negligible to more distinct clustering occurs around $St \approx 1$. This indicates that the time scale $\tau_f = L/V_0$ of the initial flow field is of physical relevance also at the early time $t = 3$. We anticipate, however, that τ_f will lose its significance as the TGV flow evolves further in time.

When the coherence of the initial large-scale TG-vortices has been broken down and the viscous energy dissipation peaks at $t \approx 9$, particles with nominal Stokes numbers $St \leq 1$ have effective Stokes numbers of order unity, except $St = 0.1$ particles for which $St_{eff} \approx 0.3$. This implies that $\tau_p \approx \tau_d$, which suggests substantial clustering. Particles with $St > 1$, however, have effective Stokes numbers $\gtrsim O(10)$, which implies that these particles respond more slowly to the local field since $\tau_p \gg \tau_d$, such that the clustering diminishes. Maximum particle clustering can be observed when the effective Stokes number is of order unity, or more specifically in the range $2 \lesssim St_{eff} \lesssim 5$. This is consistent with results reported by Balachandar et al. [36], Monchaux et al. [32] and Hogan et al. [47] who claimed that maximum particle clustering in HIT was observed for effective Stokes numbers of the order of 1.

In the second half of the simulation, i.e. beyond the peak of the energy dissipation rate at $t = 9$, the effective Stokes numbers in figure 8 decrease with time. St_{eff} becomes lower than 1 for the least inertial particles ($St \lesssim 1$), whereas $St_{eff} \lesssim 10$ for particles with intermediate inertia ($St = 3$ and 5). One should therefore anticipate that these particles are more clustered than those with even lower St. This is, however, not the case, as one can see from figure 5(b) where the particles with least inertia exhibit a higher variance σ^2. We believe that this is due to a memory effect: the finite particle response time τ_p prevents the particles to respond immediately to the new flow conditions. Inspection of figure 5(b) shows that σ^2 slowly increases beyond $t = 9$ for the particles with intermediate inertia. This

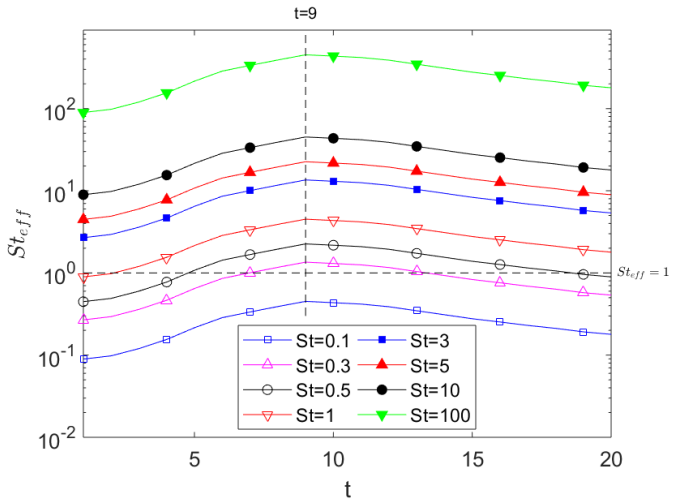

FIG. 8: Time evolution of the effective Stokes number St_{eff} defined in equation (12). The broken horizontal line $St_{eff} = 1$ corresponds to situations in which the particle response time τ_p equals the dissipation time scale τ_d of the flow.

suggests that although the effective Stokes number is decreasing with time, the anticipated increased clustering is somewhat delayed.

Generally, the most inertial particles ($St = 10$ and 100) exhibit only a modest tendency to cluster, especially at the later stages $t \geq 5$. The effective Stokes number is consistently much larger than 1, which indicates that these particles are sufficiently inertial to behave ballistically.

3. Local clustering and voids

We have seen that volume-averaged particle clustering, measured in terms of the variance σ^2 of three-dimensional Voronoï volumes, can be understood in terms of an effective Stokes number defined by means of the volume-averaged dissipation rate time scale τ_d. Let us finally look at how inertial particles concentrate in the vicinity of localized vortical structures in the TGV flow.

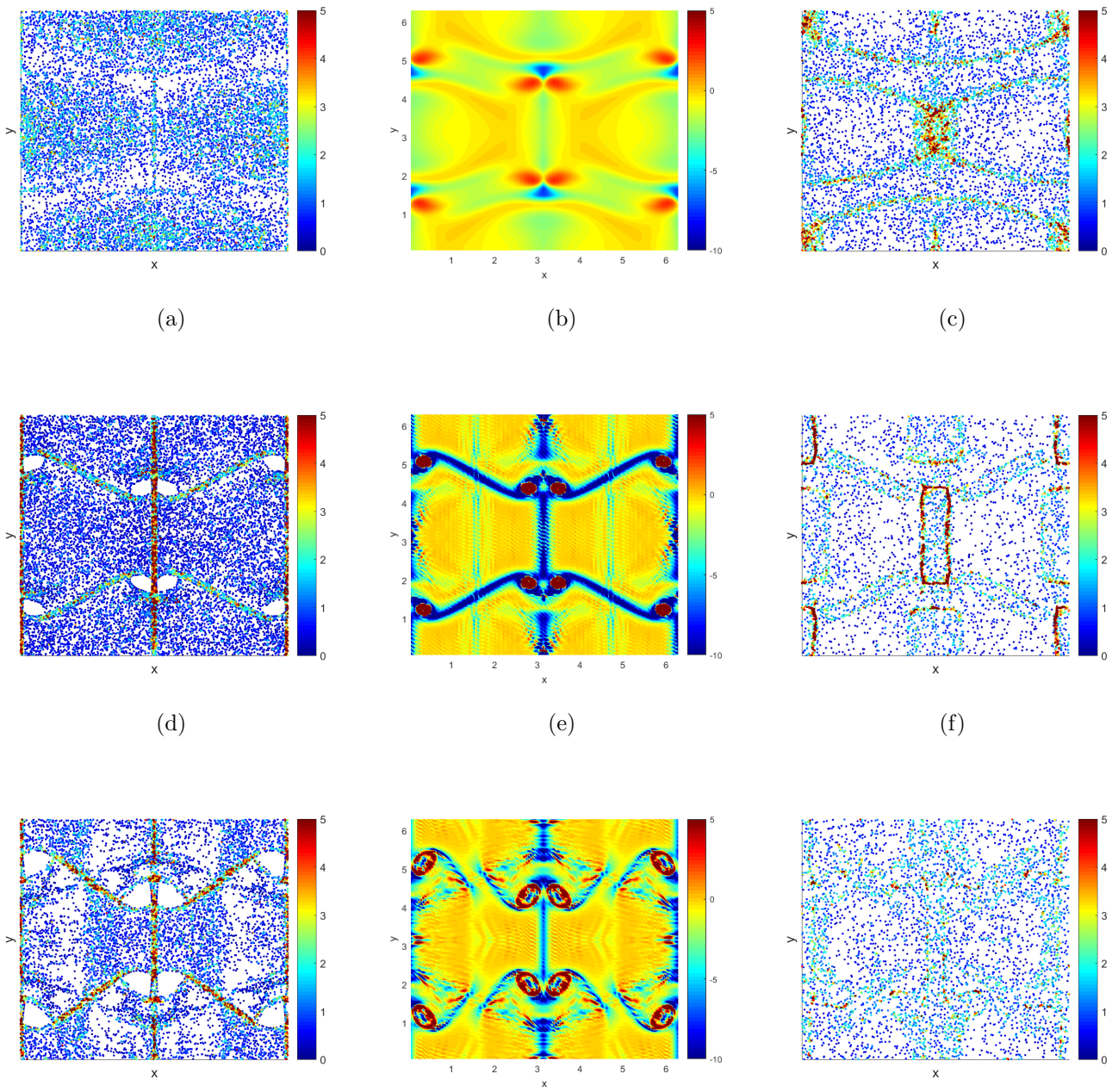

FIG. 9: Time evolution of particle and fluid fields from $t = 3$ to $t = 7$ in a (x, y)-plane. Left column: concentration of $St = 0.5$ particles; Middle column: Q-field; Right column: concentration of $St = 3$ particles.

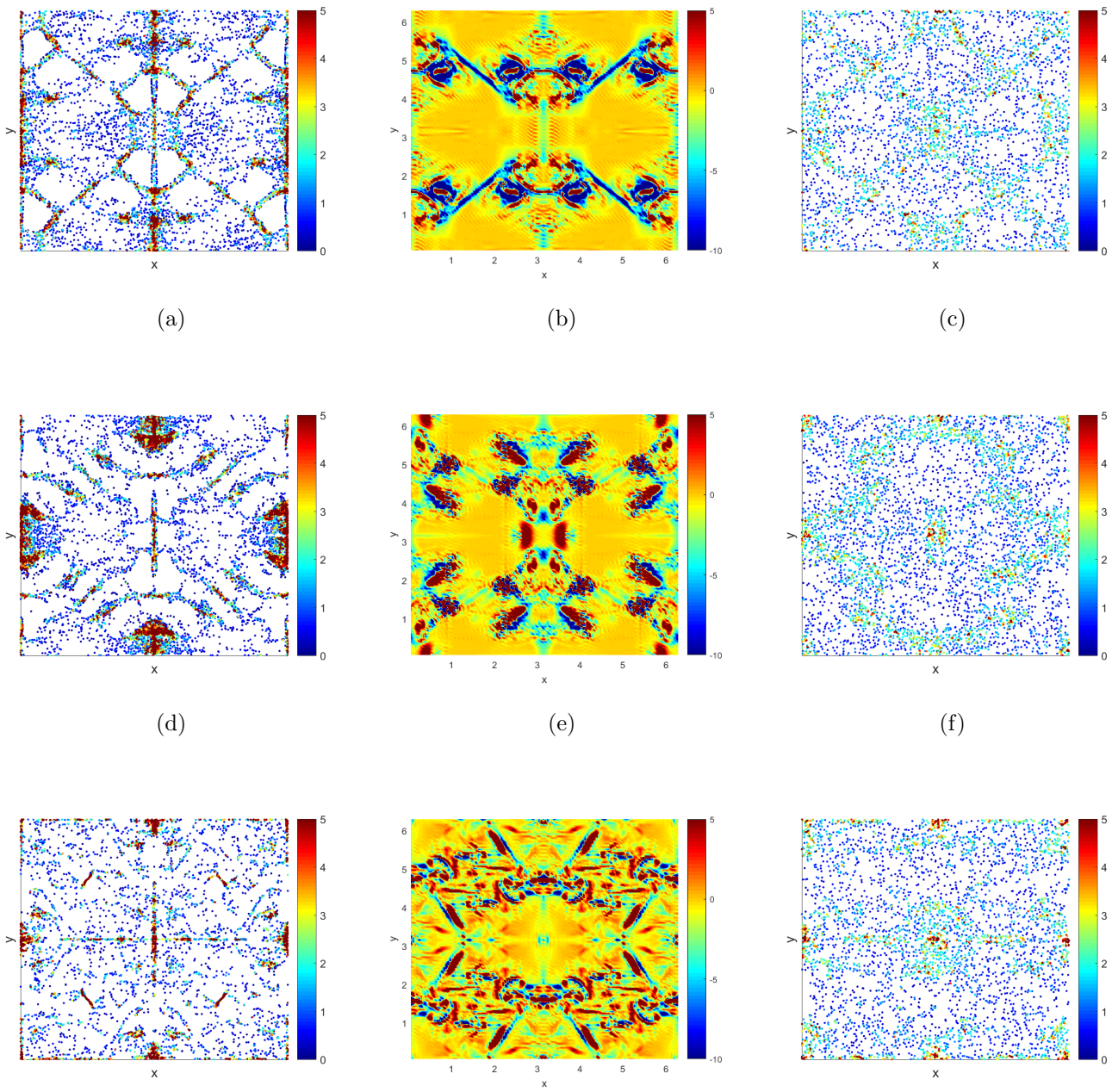

FIG. 10: Time evolution of particle and fluid fields from $t = 9$ to $t = 15$ in a (x, y)-plane. Left column: concentration of $St = 0.5$ particles; Middle column: Q-field; Right column: concentration of $St = 3$ particles.

To this end we consider the flow field and particle distributions in the (x, y)-plane at $z = \pi L$, i.e. the horizontal mid-plane. Only particles with nominal Stokes numbers 0.5 and 3 are considered first and flow and concentration fields at early times $t = 3, 5$ and 7 are shown in figure 9 and the results at later times $t = 9, 11$ and 15 are shown in figure 10. The second invariant of the velocity gradient tensor

$$Q = \frac{1}{2}[\| \Omega_{ij} \|^2 - \| S_{ij} \|^2] \tag{13}$$

is adopted as the most relevant scalar flow characteristic. Here, $\Omega_{ij} = (\partial u_i/\partial x_j - \partial u_j/\partial x_i)/2$ and $S_{ij} = (\partial u_i/\partial x_j + \partial u_j/\partial x_i)/2$ are the rotation rate and strain rate tensors, respectively. The sign of Q distinguishes between strain-rate dominated ($Q < 0$) and rotation-rate dominated ($Q > 0$) regions, see e.g. Hunt et al. [35].

Visual inspection of the plots in figures 9 and 10 shows a distinctly different behavior of particles with modest ($St = 0.5$) and intermediate ($St = 3$) inertia. The $St = 0.5$ particles are well mixed at the earliest stage at $t = 3$, but gradually start to unmix until $t = 9$, when maximum clustering can be seen. Thereafter the particles again start to mix until a fairly homogeneous particle distribution can be seen at $t = 15$. A completely different trend is seen for the $St = 3$ particles, which are clustered already at $t = 3$, in keeping with figure 5(b). The subsequent plots in figures 9 and 10 give the impression that these particles gradually become more evenly distributed as the flow evolves, at least up to $t = 9$.

The time evolution of the TGV flow has already been visualized in figure 4. Now the Q-field in the (x, y)-plane is plotted in the middle column of figures 9 and 10 at the same instants of time. The Q-contours exhibit a relatively close resemblance with the concentration contours for the $St = 3$ particles at $t = 3$ and for the $St = 0.5$ particles at the later times from $t = 5$ to 11. The $St = 0.5$ particles tend to concentrate in high strain-rate regions, i.e. $Q < 0$ (blue) and the correlation between the Q-field and the concentration field is particularly high at $t = 5$, but also at $t = 9$. These particles have an effective Stokes number close to unity during the major part of the flow development, which justifies why the particle pattern is closely linked to the vortex topology.

It is also noteworthy that the eight void areas in figure 9(d) coincide with the eight rotation-rate dominated regions, i.e. $Q > 0$ (red) in figure 9(e). Although the void areas persist for quite some time, the eight vortical structures (red) in figure 9(h) exhibit shear-rate dominated cores (blue). These $Q < 0$ zones are totally empty and demonstrate that

negative Q-values do not automatically imply high particle concentrations. Although the inertial particles are welcome to reside within these vortex cores, they are unable to penetrate through the circular $Q > 0$ barrier.

The more inertial particles with $St = 3$ behave rather differently and the concentration contours are close to the Q-field topology at $t = 3$, after which a tendency towards homogenization can be observed. At $t = 9$, for instance, the particles seem to be fairly unaffected by the Q-field. This behavior can readily be explained by the time variation of the effective Stokes number, which is around unity in the earliest stage of the flow evolvement and becomes of order 10 at time $t = 9$.

The behavior of even more inertial particles is illustrated by plots of the particle concentration in figure 11. The most inertial particles (right column) exhibit only a modest tendency to cluster, especially at the later stages $t \geq 5$, since their effective Stokes number remains consistently much larger than 1 (see figure 8 where $St_{eff} \geq 100$). The $St = 10$ particles (left column), on the other hand, exhibit characteristic clustering, which is more pronounced than that seen for the $St = 3$ particles in figure 9. At $t = 5$, for instance, the clustering pattern in figure 11(c) reveals dense clustering along the four nearly horizontal bands that correspond to $Q < 0$ in figure 9(e). Surprisingly, however, only moderate clustering can be observed along the vertical $Q < 0$ band through the center of the domain. Densely clustered particles are instead observed in an elliptical band around the center. This shows beyond any doubt that a memory effect gives rise to a major mismatch between the local Q-field and the concentration field. This is believed to be a particular feature that occurs when a particle-laden flow evolves in time.

A memory effect associated with inertial particles in an inhomogeneous flow field was discussed by Reeks [48]. He claimed that at any point the particles have some memory of their previous history – their velocity has more to do with where they came from than what is happening to the fluid motion locally. Similarly, Zhao et al. [49] argued that particles in a channel flow that are driven by turbophoresis to the near-wall region tend to concentrate in regions with locally low fluid velocity. This is understood since inertial particles do not adjust to local flow conditions, but retain their higher streamwise momentum from the channel core. These studies were both concerned with spatially inhomogeneous flows. The memory effect observed in the present study, however, is a result of the inhomogeneity in time of the evolving TGV-flow.

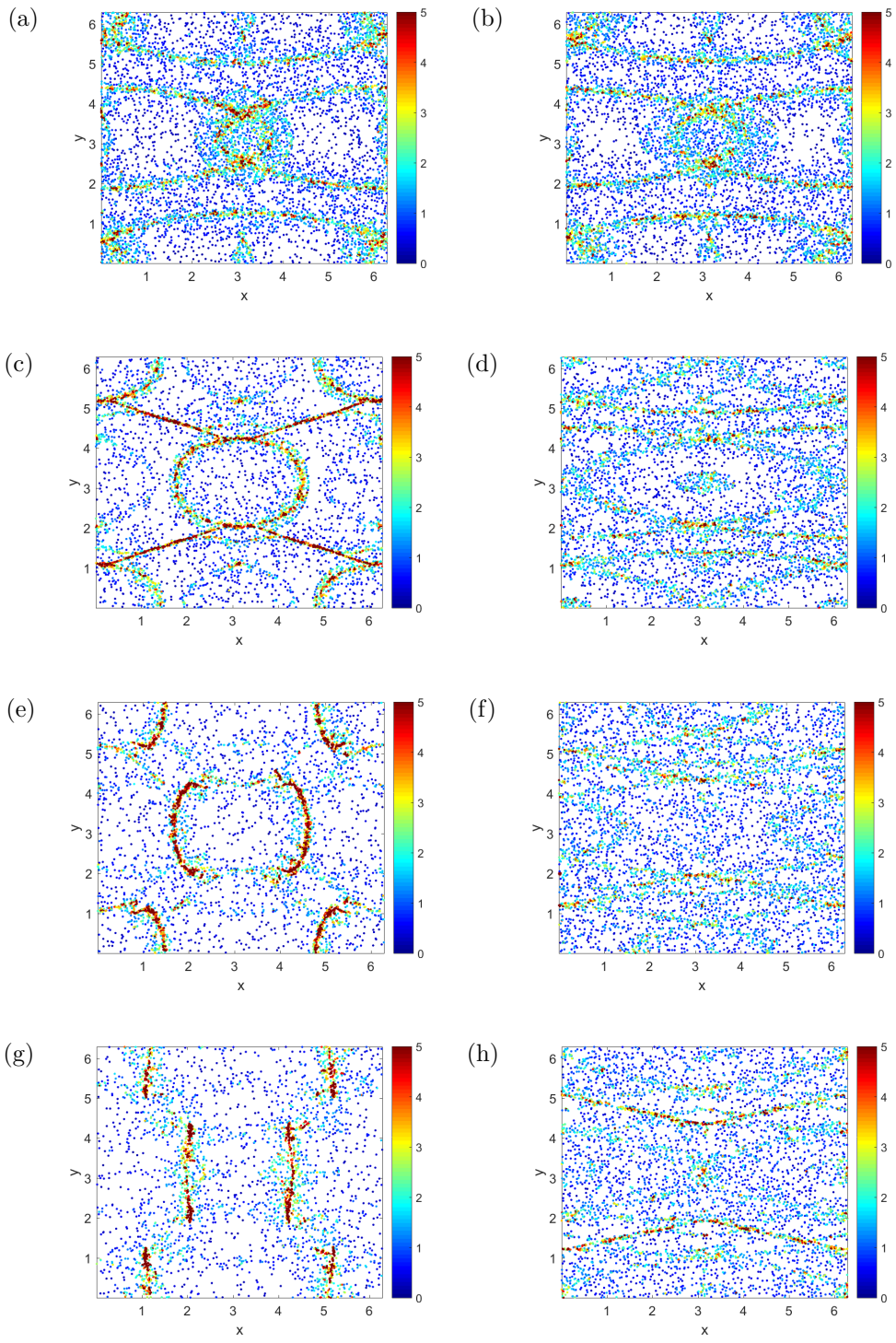

FIG. 11: Time evolution of particle fields from $t = 3$ to $t = 9$ in a (x, y)-plane. Left column: concentration of $St = 10$ particles; Right column: concentration of $St = 100$ particles.

IV. CONCLUDING REMARKS

Preferential concentration of inertial spherical particles has been studied in a continuously evolving TGV flow, in which the characteristic scales of the flow vary substantially in time. The time evolution of the flow field makes this case fundamentally different from that of particle dynamics in statistically steady flow fields, like HIT and turbulent channel flows. Although the nominal time scale $\tau_f = L/V_0$ of the initial flow field is representative in the earliest stage of the flow development, the statistical unsteadiness of the TGV flow also called for an alternative time scale. To this end we introduced the viscous dissipation time scale $\tau_d = (\nu/\epsilon)^{\frac{1}{2}}$, inspired by the Kolmogorov time scale, by means of which the effective Stokes number St_{eff} was defined.

In order to study how the clustering depended on the particle inertia, parameterized by means of the nominal Stokes number, a wide range of equal-sized inertial point-particles was considered. Voronoï tessellation was adopted to quantify the varying degree of preferential particle concentration. More specifically, the variance σ^2 of the Voronoï volumes measured the clustering.

Particles with intermediate and substantial inertia ($St > 1$) were clustered most at $t = 3\tau_f$, whereas particles with only modest inertia ($St \leq 1$) were most clustered at $t = 9\tau_f$. These findings based on σ^2 were also supported by how p.d.f.s of the Voronoï volumes compared with randomly distributed particles. This changeover from maximum clustering of $St > 1$ particles to $St \leq 1$ particles can be explained by the time variation of the characteristic flow time scale from τ_f to τ_d. Indeed, particles with nominal Stokes numbers $St \leq 1$ have attained an effective Stokes number St_{eff} of order unity at $t = 9\tau_f$ and such particles are substantially affected by the flow. This demonstrates beyond any doubt that a sound interpretation has to be based on a physically relevant time scale and its corresponding Stokes number.

Instantaneous particle concentration fields in the horizontal mid-plane at two representative Stokes numbers (0.5 and 3) showed how the particle clustering evolved in time. These planar snapshots were fully consistent with the volume-averaged σ^2. Moreover, comparisons between these particle concentrations and the corresponding Q-field contours showed that inertial particles most often tend to cluster in shear-rate dominated zones identified by negative Q-values. Maximum clustering, i.e. largest σ^2-values, corresponds to time instants

when the concentration pattern closely resembles the Q-field contours.

Finally, we also observed a memory effect, i.e. the particle concentration did not always match with the co-existing Q field. This is a consequence of the finite particle time scale τ_p, which is a measure of how efficiently a particle responds to changes in the flow field. We also observed localized strain-rate dominated areas with $Q < 0$ totally void of particles. This mismatch was ascribed to the presence of a surrounding $Q > 0$ barrier.

In summary, the observations of clustering of inertial particles in the time-evolving TGV flow are basically consistent with earlier findings in statistically steady flow fields. However, the viscous dissipation time scale changes appreciably over a few initial-flow time units L/V_0. This gives rise to a memory effect or delayed response of the particles with intermediate inertia to adapt to the scales of the surrounding flow.

ACKNOWLEDGMENTS

We would like to thank Dr. Jurriaan J.J. Gillissen for his collaboration in implementing the Sherman-Morrison algorithm. This work has been supported by The Research Council of Norway through research grant no. 250744 and computational resources through grant no. NN2694K. Y. J. and L. Z. acknowledge the support of the Natural Science Foundation of China through research grant nos. 11702158 and 91752205.

[1] G. I. Taylor and A. E. Green, Mechanism of the production of small eddies from large ones, Proc. Roy. Soc. London A **158**, 499-521 (1937).

[2] J. R. DeBonis, Solutions of the Taylor-Green vortex problem using high-resolution explicit finite difference methods, AIAA 51st Aerospace Sciences Meeting, Grapevine, Texas, AIAA-paper 0382 (2013).

[3] M. E. Brachet, D. I. Meiron, S. A. Orszag, B. G. Nickel, R. H. Morf and U. Frisch, Small-scale structure of the Taylor-Green vortex, J. Fluid Mech. **130**, 411-452 (1983).

[4] M. E. Brachet, Direct simulation of three-dimensional turbulence in the Taylor-Green vortex, Fluid Dyn. Res. **8**, 1-4 (1991).

[5] N. Sharma and T. K. Sengupta, Vortex dynamics of the three-dimensional Taylor-Green vortex

problem, Phys. Fluids **31**, 035106 (2019).

[6] T. Dairay, E. Lamballais, S. Laizet and J. C. Vassilicos, Numerical dissipation vs. subgrid-scale modelling for large eddy simulation, J. Comput. Phys. **337**, 252-274 (2017).

[7] K. D. Squires and J .K. Eaton, Preferential concentration of particles by turbulence, Phys. Fluids A **3**, 1169-1178 (1991).

[8] E. Calzavarini, M. Kerscher, D. Lohse and F. Toschi, Dimensionality and morphology of particle and bubble clusters in turbulent flow, J. Fluid Mech. **607**, 13-24 (2008).

[9] C. Marchioli and A. Soldati, Mechanisms for particle transfer and segregation in a turbulent boundary layer, J. Fluid Mech. **468**, 283-315 (2002).

[10] C. Nilsen, H. I. Andersson and L. Zhao, A Voronoi analysis of preferential concentration in a vertical channel flow, Phys. Fluids **25**, 115108 (2013).

[11] W. Yuan, L. Zhao, H. I. Andersson and J. Deng, Three-dimensional Voronoï analysis of preferential concentration of spheroidal particles in wall turbulence, Phys. Fluids **30**, 063304 (2018).

[12] L. Zhao, N. R. Challabotla, H. I. Andersson and E. A. Variano, Mapping spheroids rotation modes in turbulent channel flow: effects of shear, turbulence and particle inertia, J. Fluid Mech. **876**, 19-54 (2019).

[13] M. R. Maxey, The motion of small spherical particles in a cellular flow field, Phys. Fluids **30**, 1915-1928 (1987).

[14] L. P. Wang, M. R. Maxey, T. D. Burton and D. E. Stock, Chaotic dynamics of particle dispersion in fluids, Phys. Fluids A **4**, 1789-1804 (1992).

[15] W. M. Durham, E. Climent and R. Stocker, Gyrotaxis in a steady vortical flow, Phys. Rev. Lett. **106**, 238102 (2011).

[16] Y. Yao and J. Capecelatro, Competition between drag and Coulomb interactions in turbulent particle-laden flows using a coupled-fluid-Ewald-simulation based approach, Phys. Rev. Fluids **3**, 034301 (2018).

[17] X. Ruan, S. Chen and S. Li, Structural evolution and breakage of dense agglomerates in shear flow and Taylor-Green vortex, Chem. Eng. Sci. **211**, 115261 (2020).

[18] L. Bergougnoux, G. Bouchet, D. Lopez and E. Guazzelli, The motion of solid spherical particles falling in a cellular flow field at low Stokes number, Phys. Fluids **26**, 093302 (2014).

[19] H. Stommel, Trajectories of small bodies sinking slowly through convection cells, J. Mar. Res.

8, 24-29 (1949).

[20] S. A. Thorpe, Langmuir circulation, Annu. Rev. Fluid Mech. **36**, 55-79 (2004).

[21] W. M. Durham and R. Stocker, Thin phytoplankton layers: characteristics, mechanisms, and consequences, Annu. Rev. Marine Sci. **4**, 177-207 (2012).

[22] J. S. Guasto, R. Rusconi and R. Stocker, Fluid mechanics of planktonic microorganisms, Annu. Rev. Fluid Mech. **44**, 373-400 (2012).

[23] V. Hidalgo-Ruz, L. Gutow, R. C. Thompson and M. Thiel, Microplastics in the marine environment: a review of the methods used for the identification and quantification, Environ. Sci. Technol. **46**, 3060-3075 (2012).

[24] L. G. A. Barboza and B. C. G. Gimenez, Microplastics in the marine environment: Current trends and future perspectives, Marine Pollut. Bull. **97**, 5–12 (2015).

[25] T. S. Galloway, M. Cole and C. Lewis, Interactions of microplastic debris throughout the marine ecosystem, Nat. Ecol. Evol. **1**, 0116 (2017).

[26] L. Van Cauwenberghe, A. Vanreusel, J. Mees and C. R. Janssen, Microplastic pollution in deep-sea sediments, Environ. Pollut. **182**, 495-499 (2013).

[27] L. Van Cauwenberghe, L. Devrise, F. Galgani, J. Robbens and C. R. Janssen, Microplastics in sediments: a review of techniques, occurrence and effects, Marine Environ. Res. **111**, 5-17 (2015).

[28] L. Khatmullina and I. Isachenko, Settling velocity of microplastic particles of regular shapes, Marine Pollut. Bull. **114**, 871-880 (2017).

[29] W. M. van Rees, A. Leonard, D. I. Pullin and P. Koumoutsakos, A comparison of vortex and pseudo-spectral methods for the simulation of periodic vortical flows at high Reynolds numbers, J. Comp. Phys. **230**, 2794-2805 (2011).

[30] F. De Lillo, M. Cencini, S. Musacchio and G. Boffetta, Clustering and turbophoresis in a shear flow without walls, Phys. Fluids **28**, 035104 (2016).

[31] R. van de Weygaert and V. Icke, Fragmenting the universe. II. Voronoi vertices as Abell clusters, Astron. Astrophys. **213**, 1-9 (1989).

[32] R. Monchaux, M. Bourgoin and A. Cartellier, Preferential concentration of heavy particles: A Voronoi analysis, Phys. Fluids **22**, 103304 (2010).

[33] R. Monchaux, M. Bourgoin and A. Cartellier, Analyzing preferential concentration and clustering of inertial particles in turbulence, Int. J. Multiphase Flow **40**, 1-18 (2012).

[34] M. García-Villalba, A. G. Kidanemariam and M. Uhlmann, DNS of vertical plane channel flow with finite-size particles: Voronoi analysis, acceleration statistics and particle-conditioned averaging, Int. J. Multiphase Flow **46**, 54-74 (2012).

[35] J. C. R. Hunt, A. A. Wray and P. Moin, Eddies, streams, and convergence zones in turbulent flows, Center Turbul. Res. Rep. CTR-S88, 193-208 (1988).

[36] S. Balachandar and J. K. Eaton, Turbulent dispersed multiphase flow, Annu. Rev. Fluid Mech. **42**, 111-133 (2010).

[37] S. Sundaram and L. R. Collins, Collision statistics in an isotropic particle-laden turbulent suspension. Part 1. Direct numerical simulations, J. Fluid Mech. **335**, 75-109 (1997).

[38] J. Bec, L. Biferale, G. Boffetta, A. Celani, M. Cencini, A. Lanotte, S. Musacchio and F. Toschi, Acceleration statistics of heavy particles in turbulence, J. Fluid Mech. **550**, 349-358 (2006).

[39] N. Egidi and P. Maponi, A Sherman-Morrison approach to the solution of linear equations, J. Comput. Appl. Math. **189**, 703-718 (2006).

[40] R. Jayaram, J. J. J. Gillissen, L. Zhao and H. I. Andersson, Numerical solution of Poisson equation using Sherman-Morrison algorithm in Taylor-Green vortex flow, In Proceedings of 10^{th} National Conference on Computational Mechanics, Trondheim, Norway, CIMNE, 197-210 (2019).

[41] D. Mitra, N. E. L. Haugen and I. Rogachevskii, Turbophoresis in forced inhomogeneous turbulence, Eur. Phys. J. Plus **133**, 35 (2018).

[42] L. Schiller and A. Z. Naumann, Über due grundlegenden Berechnungen bei der Schwerkraft aufereitung, Z. Ver. Deutch. Ing. **77**, 318-320 (1933).

[43] P. H. Mortensen, H. I. Andersson, J. J. J. Gillissen and B. J. Boersma, Particle spin in a turbulent shear flow, Phys. Fluids **19**, 078109 (2007).

[44] L. Zhao, H. I. Andersson and J. J. J. Gillissen, Turbulence modulation and drag reduction by spherical particles, Phys. Fluids **22**, 081702 (2010).

[45] L. Zhao, C. Marchioli and H. I. Andersson, Stokes number effects on particle slip velocity in wall-bounded turbulence and implications for dispersion models, Phys. Fluids **24**, 021705 (2012).

[46] J. S. Ferenc and Z. Néda, On the size distribution of Poisson Voronoi cells, Physica A **385**, 518-526 (2007).

[47] R. C. Hogan and J. N. Cuzzi, Stokes and Reynolds number dependence of preferential particle concentration in simulated three-dimensional turbulence, Phys. Fluids **13**, 2938-2945 (2001).

[48] M. W. Reeks, Transport, mixing and agglomeration of particles in turbulent flows, Flow Turbulence Combust. **92**, 3-25 (2014).

[49] L. Zhao, H. I. Andersson and J. J. J. Gillissen, Interphasial energy transfer and particle dissipation in particle-laden wall turbulence, J. Fluid Mech. **715**, 32-59 (2013).